RESEARCH ARTICLE

[18F]Amylovis as a Potential PET Probe for β-Amyloid Plaque: Synthesis, *In Silico*, *In vitro* and *In vivo* Evaluations
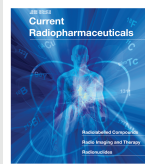
Suchitil Rivera-Marrero[a], Laura Fernández-Maza[b], Samila León-Chaviano[a], Marquiza Sablón-Carrazana[a], Alberto Bencomo-Martínez[a], Alejandro Perera-Pintado[c], Anais Prats-Capote[c], Florencia Zoppolo[d], Ingrid Kreimerman[d], Tania Pardo[d], Laura Reyes[d], Marcin Balcerzyk[b], Geyla Dubed-Bandomo[a], Daymara Mercerón-Martínez[a], Luis A. Espinosa-Rodríguez[e], Henry Engler[d], Eduardo Savio*[d] and Chryslaine Rodríguez-Tanty*[a]

aDepartment of Neurochemistry, Cuban Center for Neurosciences, Havana, Cuba; bCentro Nacional de Aceleradores, Parque Científico y Tecnológico Cartuja, Seville, Spain; cCenter of Isotopes (CENTIS), Mayabeque, Cuba; dRadio-pharmacy R&D, Uruguayan Center of Molecular Imaging (CUDIM), Montevideo, Uruguay; eCenter of Genetic Engine-ering and Biotechnology (CIGB), Havana, Cuba.

Abstract. *Background*: Alzheimer's disease (AD) is the most common form of dementia. Neuroimaging methods have widened the horizons for AD diagnosis and therapy. The goals of this work are the synthesis of 2-(3-fluoropropyl)-6-methoxynaphthalene (**5**) and its [18F]-radiolabeled counterpart ([18F]Amylovis), the in silico and in vitro comparative evaluations of [18F]Amylovis and [11C]Pittsburg compound B (PIB) and the in vivo preclinical evaluation of [18F]Amylovis in transgenic and wild mice.

Methods: Iron-catalysis cross coupling reaction, followed by fluorination and radiofluorination steps were carried out to obtain **5** and 18F-Amylovis. Protein/Aß plaques binding, biodistribution, PET/CT Imaging and immunohistochemical studies were conducted in healthy/transgenic mice.

Results: The synthesis of **5** was successful obtained. Comparative in silico studies predicting that 5 should have affinity to the Aβ-peptide, mainly through π-π interactions. According to a dynamic simulation study the ligand-Aβ peptide complexes are stable in simulation-time (ΔG = -5.31 kcal/mol). [18F]Amylovis was obtained with satisfactory yield, high radiochemical purity and specific activity. The [18F]Amylovis log $P_{oct/PBS}$ value suggests its potential ability for crossing the blood brain barrier (BBB). According to in vitro assays, [18F]Amylovis has an adequate stability in time. Higher affinity to Aβ plaques were found for [18F]Amylovis (K_d 0.16 nmol/L) than PIB (K_d 8.86 nmol/L) in brain serial sections of 3xTg-AD mice. Biodistribution in healthy mice showed that [18F]Amylovis crosses the BBB with rapid uptake (7 %ID/g at 5 min) and good washout (0.11±0.03 %ID/g at 60 min). Comparative PET dynamic studies of [18F]Amylovis in healthy and transgenic APPSwe/PS1dE9 mice, revealed a significant high uptake in the mice model.

Conclusion: The in silico, in vitro and in vivo results justify that [18F]Amylovis should be studied as a promissory PET imaging agent to detect the presence of Aβ senile plaques.

Keywords: Alzheimer's disease diagnosis, positron emission tomography, β-amyloid probe, fluorine-18, iron cross-coupling reaction, docking and dynamic simulations.

1. INTRODUCTION

The pathophysiological process of dementia associated with Alzheimer's disease (AD) begins years, if not decades, before cognitive impairment and clinical diagnosis [1, 2]. This process starts with the accumulation of senile plaques (SPs), mainly constituted by the amyloid β 1-42 (Aβ1-42) peptide, which eventually leads to neuroinflammatory changes, synaptic dysfunction, and finally, to neuronal degeneration [3]. The long preclinical phase of AD provides a critical opportunity for potential intervention with disease-modifying therapies. Then, finding out an early diagnosis for this disease constitutes a challenge to the scientific community [4, 5].

Around 25.5 million of people worldwide suffered from dementia in 2000, with a prognosis of 75 million in 2030 and 131 million in 2050, representing AD the most common type of dementia, accounting for 60-70% of all the cases [6]. As the number of patients with AD will increase in the future,

*Address correspondence to this author at Radiopharmacy R&D, Uruguayan Center of Molecular Imaging (CUDIM), Montevideo, Uruguay; Tel: 598-24803238; Ext: 122; E-mail: eduardo.savio@cudim.org

the burden on society for the healthcare of these patients will be enormous.

One of the most promising ways for direct mapping of Aβ plaques in the living brain has been the development of imaging agents, using neuroimaging techniques such as Magnetic Resonance Imaging (MRI) [7, 8], Single-Photon Emission Computed Tomography (SPECT) [9] and Positron Emission Tomography (PET) [10]. Some compounds labeled with positron-emitter radionuclides have been studied as radiopharmaceuticals for detection of senile plaques (SPs) in AD patients [11], such as: styrylbenzenes, benzothiazoles, stilbenes, vinyl benzoxazoles, naphthalene derivatives and others [12]. Mostly, the synthetic procedures to obtain these compounds are complex. In general, radiotracers should accomplish some properties to be used for the *in vivo* detection of Aβ plaques. For instance, they must have a high *in vitro* binding affinity (K_i < 10 nM), a high permeability (log P < 3) to Blood-Brain Barrier (BBB), a high initial brain uptake with rapid clearance in the normal brain, and also they must have a very high ratio of specific to nonspecific binding in the brain [7]. Furthermore, the labeling procedures should be efficient [13]. In the last years, the Food and Drug Administration (FDA) has approved three PET radiopharmaceuticals for the visualization of Aβ deposits in AD brains three as below mentioned compounds: [¹⁸F]Florbetapir ([¹⁸F]AV-45, Amyvid, 2012) [14], [¹⁸F]Flutemetamol ([¹⁸F]GE-067, Vizamyl, 2013) [15] and [¹⁸F]Florbetaben ([¹⁸F] BAY94-9172, Neuraceq, 2014) [16] . However, the detection of Aβ plaques in early stages by PET is still a challenge [10, 17]. Therefore, in the field of PET neuroimaging, the design and development [¹⁸F]-PET probes are not a concluded task yet. Reaching this goal would increase the potential applications of this technique.

In our study, the synthesis of 2-(3-fluoropropyl)-6-methoxynaphthalene and its [¹⁸F]-radiolabeled counterpart ([¹⁸F]Amylovis), through a simple and suitable procedure, was reported. *In silico* and *in vitro* evaluations of [¹⁸F]Amylovis in comparison with [¹¹C]Pittsburg compound B (PIB) were done to explore the affinity of this new radiolabeled compound towards Aβ plaques. Finally, *in vivo* preclinical evaluation of [¹⁸F]Amylovis in transgenic and wild mice was carried out.

2. EXPERIMENTAL

2.1. Organic Synthesis

2.1.1. General

All chemicals and reagents were obtained from commercial suppliers. Analytical TLC was performed on silica gel 60 F_{254} (Merck, Germany), using benzene as a mobile phase. Silica gel (Silica 60, 230-400 mesh, Merck) was used to carry out chromatographic columns. IR spectra were recorded on a Beijing Rayleigh Analytical Instrument Corp. FTIR-WQF-510 spectrophotometer. NMR spectra were recorded on a Bruker Model AC 250F, JEOL ECLIPSE 400 and Bruker DPX-400 spectrometers. The chemical shifts assignment was based on standard NMR experiments (¹H, ¹H-COSY, HSQC, HMBC and ¹³C NMR). The chemical shift values were expressed in ppm. Melting points were determined on an Electrothermal (model 9100, UK) equip-

ment. Mass spectra were determined on a hybrid mass spectrometer with orthogonal geometry QTOF-2 (Micromass, UK) with electrospray ionization (ESI-MS).

2.1.2. Synthesis of Naphthalene Derivatives

2.1.2.1. 6-bromo-2-naphthol (1)

6-bromo-2-naphthol was synthesized according to [18]. Yield: 95% (reported 96%) [18], m.p: 123.3-127.7°C (reported 120-124°C) [18]. Rf: 0.28. ¹H-NMR ($CDCl_3$/325 K, ppm): 7.94-7.90 (1H, d, CH_{arom}-1); 7.68-7.64 (1H, d, CH_{arom}-8); 7.60 (1H, d, CH_{arom}-4); 7.49-7.43 (1H, t, CH_{arom}-3); 7.31-7.25 (1H, t, CH_{arom}-5); 7.17-7.14 (1H, d, CH_{arom}-7); 5.82 (1H, s, OH). ¹³C-NMR ($CDCl_3$/325 K): 150.56 (C-2, c); 132.28 (C_{arom}-9, c); 129.67(C_{arom}-10, c); 129.30 (CH_{arom}-8, t); 128.19 (CH_{arom}-1, t); 127.81 (CH_{arom}-3, t); 125.30 (CH_{arom}-4, t); 124.11 (CH_{arom}-7, t); 117.13 (CH_{arom}-2, C); 106.12 (C_{arom}-6, c).

2.1.2.2. 6-bromo-2-methoxynaphthalene (2)

6-bromo-2-methoxynaphthalene was synthesized according to [18]. Yield: 83% (reported 85%) [18], m.p: 105-106.5°C (reported 103-105°C) [18]. Rf: 0.63. ¹H-NMR ($CDCl_3$/325 K, ppm): 7.90 (1H, d, CH_{arom}-1); 7.65 (1H, m, CH_{arom}-8); 7.58 (1H, m, CH_{arom}-4); 7.51 (1H, m, CH_{arom}-3); 7.18 (1H, m, CH_{arom}-5); 7.08 (1H, m, CH_{arom}-7); 3.91 (3H, s, CH_3O-). ¹³C-NMR ($CDCl_3$/325 K, ppm): 157.88 (C-2, c); 133.04 (C_{arom}-9, c); 130.01 (C_{arom}-10, c); 129.65 (CH_{arom}-8, t); 129.61 (CH_{arom}-1, t); 128.48 (CH_{arom}-3, t); 128.36 (CH_{arom}-4, t); 119.75 (CH_{arom}-7, t); 117.02 (C_{arom}-6, c); 105.77 (CH_{arom}-5, t); 55.32 (CH_3O-, p).

2.1.2.3. bromo(6-methoxy-2-naphthyl)magnesium (3)

A round-bottom flask (50 mL), equipped with a magnetic stirring bar and pressure equalizing funnel, was sealed with a rubber septum. Then, the air was evacuated and refilled four times with anhydrous argon. Magnesium turnings (61 mg, 2.5 mmol) and a speck of iodine were suspended in anhydrous THF (1.5 mL) and later, several drops of **2** (600 mg, 2.5 mmol) in THF (5 mL) were added. The reaction mixture was refluxed to initiate the reaction and when it became cloudy; the remaining of **2** solution was added dropwise and refluxed for 2 h additional.

2.1.2.4. General Procedure for Obtaining 3-(6-methoxy-2-naphthyl)propyl-4-methylbenzenesulfonate (4) by Cross-Coupling Reactions

A round-bottom flask (50 mL), equipped with a magnetic stirring bar and pressure equalizing funnel, was sealed with a rubber septum, then evacuated and refilled four times with anhydrous argon. The flask was charged with 1,3-propanediol di-*p*-tosylate (DiTs, 711 mg, 1.87 mmol), catalyst (5 mol%, see Table **1**) and co-ligand (Table **1**), and then anhydrous THF (11 mL) was added. This solution was stirred for 5 min and later, bromo(6-methoxy-2-naphthyl)magnesium (2.5 mmol, 6.25 mL anhydrous THF, 0.4 mol/L) was slowly added to the reaction mixture during 4 hours, at the selected temperature (Table **1**). The reaction mixture was vigorously stirred at room temperature for an additional 24 h. During the reaction, a color change from red

to green was observed. The reaction was quenched with NH$_4$Cl saturated solution (6 mL). Standard extractive work-up followed by flash chromatography of the crude product (cyclohexane: hexane, from 1:0 to 1:1, v/v) provided **4**, as a white solid (402 mg, 1.08 mmol, 43%, purity 98%). Rf: 0.36. IR (KBr/cm^{-1}): 3050.83, 3004.55 (ν Csp$_2$-H); 2929.34, 2848.35 (ν Csp$_3$-H); 1604.48, 1484.92 (ν C=C); 1390.42 (δ CH$_3$); 1346.07, 1172.51 (ν SO$_2$); 1230.36, 1031.73 (ν C-O-CH$_3$). ^{1}H-NMR (CDCl$_3$/325 K, ppm): 7.73-7.67 (2H, m, CH$_{arom}$); 7.52-7.50 (2H, dd, CH$_{arom}$); 7.33 (1H, s, CH$_{arom}$); 7.22-7.19 (2H, m, CH$_{arom}$); 7.10-7.01 (3H, m CH$_{arom}$); 3.96 (2H, t,CH$_2$OTs); 3.80 (3H, s, CH$_3$O-); 2.68 (2H, t, CH$_2$-Naph); 2.32 (3H, s, CH$_3$-Ts), 1.98-1.87 (2H, q, CH$_2$-$_{int}$). ^{13}C-NMR (CDCl$_3$/325 K, ppm): 157.45 (C$_{arom}$-6, c); 144.77 (C$_{Ts}$-C-CH$_3$, c); 135.56 (C$_{arom}$-9, c); 133.33 (C$_{Ts}$-C-SO$_2$O, c); 133.25 (C$_{arom}$-10, c); 129.91 (2 CH$_{Ts}$ BB′, t); 129.13 (C$_{arom}$, c); 128.96 (C$_{arom}$-8, t); 127.95 (2 CH$_{arom-Ts}$AA′, t), 127.56 (CH$_{arom}$, t); 127.06 (CH$_{arom}$, t); 126.55 (CH$_{arom}$, t); 118.85 (CH$_{arom}$-7, t); 105.86(CH$_{arom}$-4, t); 69.73 (CH$_2$O-Ts, s); 55.37 (CH$_3$O-Naph, p); 31.46 (CH$_2$-Naph,s); 30.47 (CH$_2$-CH$_2$, s); 21.65 (CH$_3$-Ts, p). ESI-MS (m/z): calc. for C$_{21}$H$_{22}$O$_4$S: 370.46, found 371.14 (M+1)$^+$.

2.1.2.5. 2-(3-fluoropropyl)-6-methoxynaphthalene (5)

To a solution of **4** (370 mg, 1 mmol), in *tert*-amylic alcohol (4 mL), tetra-*n*-butylammonium fluoride (TBAF, 298 mg, 1 mmol) was added. The resulting mixture was stirred for 24 h, at 70 °C. Then, the solvent was removed under vacuum. The syrup was washed with distilled water (5 mL) and the organic compound was extracted with ethyl acetate (5 mL x 3). Standard extractive work-up followed by flash chromatography of the crude product was carried out (hexane: cyclohexane, 1:1) (198 mg, 0.91 mmol, 91%, purity 97%). Rf: 0.6. IR (KBr/cm^{-1}): 3056.62, 3004.55 (ν Csp$_2$-H); 2960.20, 2937.06, 2852.20 (ν Csp$_3$-H); 1604.48, 1506.13, 1484.92 (ν C=C); 1392.35 (δ CH$_3$); 1230.36, 1029.80 (ν C-O-CH$_3$); 1159.01 (ν C-F). ^{1}H-NMR (CDCl$_3$/325 K, ppm): 7.69 (1H, s, CH$_{arom}$-8); 7.67 (1H, s, CH$_{arom}$-4); 7.57 (1H, s, CH$_{arom}$-1); 7.32-7.26 (1H, m, CH$_{arom}$-3); 7.15-7.12 (2H, m, CH$_{arom}$ -7 and -5); 4.55 (1H, d, CH$_2$-F, ^{2}J= 47.24); 4.43 (1H, d, CH$_2$-F, ^{2}J= 47.24); 3.92 (3H, s, CH$_3$O-); 2.88 (2H, t, CH$_2$-Naph); 2.17-2.04 (2H, m, -CH$_2$-$_{int}$). ^{13}C-NMR (CDCl$_3$/325 K, ppm): 157.40 (C$_{arom}$-6,c); 136.35 (C$_{arom}$-2, c); 133.21 (C$_{arom}$-9, c); 129.21 (C$_{arom}$-10, c); 129.05 (CH$_{arom}$-8, t); 127.84 (CH$_{arom}$-3, t); 127.06 (CH$_{arom}$-4, t); 126.62 (CH$_{arom}$-1, t); 118.94 (CH$_{arom}$-7, t); 105.76 (CH$_{arom}$-5, t); 84,11 and 82,47 (CH$_2$-F,s, ^{1}J= 164.66); 55.44 (CH$_3$O-, p); 32.26 and 32.07 (CH$_2$-$_{int}$,s, ^{2}J= 19.76); 31.40 and 31.34 (CH$_2$-Naph,s, ^{3}J= 5.86). ESI-MS (m/z): calc. for C$_{14}$H$_{15}$FO: 218.27, found 219.14 (M+H)$^+$.

2.2. In silico Studies

2.2.1. Molecular Docking

The 3D-NMR structure of the Aβ$_{1-42}$ amyloid peptide was downloaded from the PDB (1IYT code) [19]. The structures of **5** and PIB were refined using Avogadro software [20] and converted into .pdbqt format with Autodock Tools, considering all ligand bonds as flexible. These compounds were blindly docked with Aβ$_{1-42}$ peptide using AutoDockVina [21]. The conformers with the lowest binding energy were

calculated from 10 different conformations for each docking simulation between the peptide and the ligands, at 5 Å distance. For these simulations, all amino acids of the evaluated protein were considered in a rigid position. The folder with the data for calculation was compiled in a file, which contained the Aβ$_{1-42}$ configurations (.pdbqt) and the corresponding ligand configuration (.pdbqt). The selected values for the center of coordinates of the box were -1, 0, and 1 Å on the x, y, z-axis respectively, and the dimensions for each of the axes were 60, 60 and 70 Å. Thus, the ligand can move freely across the surface of the Aβ$_{1-42}$. The visualization and determination of the interaction zones between the amino acids and the tested compound were carried out using the molecular graphics program Pymol. The scoring function values were obtained from AutodockVina. Low root-mean-square-deviation (RMSD) values were obtained in all assays. All calculations were performed on a cluster of 10 computers (30 CPU) using Linux as an operating system.

2.2.2. Molecular Dynamics Simulations

Molecular dynamics simulations were performed using GROMACS 4.6.5 [22] based on the docked conformation of **5** and amyloid peptide. An Amber 99SB force field was used for protein parameters [23]. Three Na$^+$ ions were added to neutralize the system and then solvated in a dodecahedron box of spc (simple point charge) water molecules. The PRODRG 2.5 [24] (available in the PRODRG website: http://davapc1.bioch.dundee.ac.uk/cgi-bin/prodrg) were used to generate all ligand parameters. To relieve any geometric strain and close intermolecular contacts, the ligand-peptide complex was subjected to previous steps of energy minimization and solvent and ions were equilibrated around amyloid peptide. Equilibration was conducted in two phases: NVT and NPT. In the NVT phase (constant number of particles, volume, and temperature), a weak constraint to the system was impose (10 kcal/mol) and was gradually heated from 0 to 300 K in 100 ps and then equilibrated for 100 ps at 300 K. In the NPT phase (constant number of particles, pressure, and temperature) the system was equilibrated for 100 ps at 300 K. A molecular dynamics simulations of 30 ns were performed with constant pressure (1 atm), temperature (300 K) and using periodic boundary conditions. 300 trajectory structures were obtained for subsequent analysis and the equilibration was monitored by examining the stability potential energy and the RMSD calculations between amyloid peptide backbone and each ligand.

2.3. Radiolabeling. Fully Automated Radiosynthesis

2.3.1. Radiosynthesis of 2-(3-[^{18}F]fluoropropyl)-6-methoxy naphthalene ([^{18}F]Amylovis)

[^{18}F]fluoride ion was produced in the cyclotron via the nuclear reaction ^{18}O(p,n)^{18}F. It was delivered as a solution in [^{18}O]H$_2$O to an automated synthesis module GE TRACERlab$^®$ FX-FN. This solution was trapped on an anion exchange cartridge (QMA). The [^{18}F]fluoride was eluted to the reactor by a mixture of aqueous potassium carbonate (3.5 mg in 100 μL of water) and Kryptofix [2.2.2] (15 mg in 900 μL of acetonitrile). The solution was dried by azeotropic distillation at 65°C for 5 min. Once the solvents were removed the precursor **4** (1.0 mg) in 1.0 mL of anhydrous acetonitrile was

added to the dried [^{18}F]fluoride. The reactor was then heated at 70 °C for 10 minutes to obtain 2-(3-[^{18}F]fluoropropyl)-6-methoxynaphthalene ([^{18}F]Amylovis). Afterwards, the crude reaction mixture was cooled to 40 °C, transferred to a pre-injection vial and then diluted with 2 mL of the semi-preparative HPLC eluent (MeCN:H$_2$O (70:30)). The HPLC purification was performed using a C18 semi-preparative column and the mobile phase mentioned above at a flow rate of 4 mL/min. Chromatograms were registered using a UV (λ= 220 nm) and a gamma *in-line* detectors. The desired product was collected between 11 and 13 min and diluted with 50 mL of water for injection into a collection flask. This solution was again purified through a C18light-SPE cartridge, pre-activated with 1 mL of absolute ethanol followed by 10 mL of water for injection. The cartridge was washed with 10 mL of water for injection. The trapped product was eluted with 1 mL of absolute ethanol. Finally, formulation was done with 5.2 mL of 0.9% NaCl, 500 µL of Na$_2$HPO$_4$ (0.1 mmol/L, pH 8.5) and 350 µL of a solution of Tween 80 (0.11 mmol/L in 0.9% NaCl). The final solution was transferred to a sterile vial through a 0.20 µm hydrophilic sterilizing filter and used in all assays.

2.3.2. Quality Control

Chemical and radiochemical purities were assessed by analytic RP-HPLC, with MeCN:H$_2$O (75:25) as mobile phase, flow rate of 1 mL/min on a C18 column. Chromatograms were registered using UV (λ= 215 nm) and gamma detectors in series. The retention time of the precursor and the product were 11.0 and 8.4 min, respectively. Radiochemical identity was determined by comparing the retention time of the product with the nonradioactive reference standard. The radiochemical purity was determined integrating the area corresponding to the [^{18}F]Amylovis´s peak in relation to the total radioactivity. Specific activity was calculated as the relation between the product activity at the end of synthesis and the amount of the unlabelled compound. Quality control of three different batches is summarized in Supplementary Material, Table **1S**).

2.3.3. Lipophilicity

The [^{18}F]Amylovis partition coefficient was determined in *n*-octanol (2 mL) and phosphate buffer (2 mL, 0.1 mol/L, pH 7.4). The two phases were pre-saturated with each other. [^{18}F]Amylovis (100 µL) was added and the mixture was shaken by vortex for two minutes and centrifuged at 5 000 rpm for 5 min at 4°C. Subsequently, the two phases were separated and three samples (50 µL) of each phase were taken and their activity measured in a solid scintillation counter. Three replicates were performed and each one in triplicate. The partition coefficient was calculated using:

log P: log (counts in octanol/ counts in buffer).

2.4. *In vitro* Studies

2.4.1. *[¹⁸F]Amylovis Stability in the Final Formulation*

Three samples of final formulation of [^{18}F]Amylovis were evaluated at different times (0, 1, 2, 3, 4, 5 and 6h) at room temperature. These samples were analyzed by analytical radio-HPLC using the conditions described in quality control.

2.4.2. Stability in Plasma

1 mL of human plasma was incubated with 100 µL of [^{18}F]Amylovis at 37ºC for 2 hours. Plasma samples (100 µL) were taken at different incubation times (30, 60, 90 and 120 minutes). Plasma samples were extracted with 150 µL of absolute ethanol, at -15ºC, and mixed with a vortex to denaturalize the proteins. To precipitate proteins the mixtures were centrifuged (2 minutes, 5000 rpm at 4ºC). The supernatants were analyzed by radio-HPLC.

2.4.3. Protein Binding Assay

Molecular exclusion columns (Microspin TM G-50, GE Healthcare) were prepared by centrifugation (2 minutes, 3300 rpm at 4ºC). 1 mL of human plasma was incubated with 100 µL of [^{18}F]Amylovis at 37ºC for 120 minutes. 50 µL of plasma samples were applied to the columns at different incubation times (30, 60 and 120 minutes) and incubated for 2 minutes. The columns were centrifuged (2 min, 3300 rpm at 4ºC) and eluates were collected. The radioactivity of columns (corresponding to free compound) and eluates (corresponding to binding compound) were measured by a gamma counter. A blank was carried out at 120 minutes of incubation, replacing plasma for 0.1 M phosphate buffer.

2.4.4. In vitro Binding Assays with Aβ Plaques

The binding assays were carried out by *in vitro* autoradiographic studies using *post-mortem* brain serial axial sections (10 µm) of homozygous 3xTg-AD mice (B6; 129Psen1tm1MpmTg(APPSwe, tauP301L)1Lfa/Mmjax, 9 months, female). Brain serial axial sections, over borosilicate glass, were pre-incubated for 10 min at room temperature in Tris-Mg buffer (tris-HCl 0.05 mol/L, pH 7; 45 mmol/L MgCl$_2$ and 0.002 % BSA), before testing.

The equilibrium dissociation constant values (K$_d$) of the [^{18}F]Amylovis and [^{11}C]PIB binding to Aβ plaques were determined according to [25, 26]. Briefly, the brain serial sections were incubated with increasing concentrations of [^{11}C]PIB (0.05, 0.1, 0.2, 0.25, 0.3, 0.4, 0.5 MBq/mL), or [^{18}F]Amylovis (0.005, 0.01, 0.04, 0.07, 0.1 MBq/mL), by triplicate, during 40 or 120 min, respectively. Nonspecific binding was defined in the presence of **5** (10000 nmol/L). The sections were dipped for rising in cold Tris-Mg buffer for 3 min, three times, and then one time in bi-distilled water for 30 s. Later, the slides containing dry sections were exposed to BAS-IP MR 2040 imaging plate (Fuji Film, Tokyo, Japan) overnight. Autoradiographic images were obtained using an HS screen, images acquired on a PhosphorImager and analyzed using a computer-based image analysis system (Image Quant TL). The maximum binding sites (Bmax) and dissociation constant (K$_d$) of the [^{18}F]Amylovis and [^{11}C]PIB were calculated by non-linear regression analysis and Scatchard analyses [26] from binding data, respectively, using GraphPad Prism software version 5.00 (San Diego, CA).

2.5. *In vivo* Studies

2.5.1. Biodistribution Study

Thirty healthy male Balb/C mice of 10-12 weeks and 28.5±2.0 g were divided into 6 groups of 5 animals each. A dose of 20-40 MBq of [^{18}F]Amylovis was intravenously ad-

ministered through a lateral tail vein. Blood samples were collected and the animals were sacrificed at 5, 15, 30, 45, 70 and 180 min after injection. Organs of interest were removed, washed with saline, dried and weighted. Radioactivity of blood, plasma, urine, faeces, brain, cerebellum, heart, liver, stomach, spleen, large intestine, small intestine, left kidney, muscle (thigh), bone (femur) and tail was measured in a well counter. Pharmacokinetic parameters (area under the drug concentration curve, AUC; plasma half-life, $T_{1/2}$; maximal plasma concentration, C_{max}; clearance, Cl; volume of distribution at steady state, Vss) were calculated by non-compartmental analysis (NCA) using Winnolin 6.0 software (Pharsight, USA). Mean value and standard deviation of determined parameters were reported.

2.5.2. PET/CT Imaging Studies

Small animal PET/CT imaging studies were conducted in male C57BL/6 mice (nine animals, aged: 13 months) and in male transgenic APPSwe/PS1dE9 mice (nine animals, aged 12 months) [27]. Animals were anaesthetized with 4-5% isoflurane (maintenance 1-2 %) for all the studies they were involved. All applicable international and national guidelines for the care and use of animals were followed. All procedures performed in studies involving animals were carried out in compliance with national regulation of Spain relating to conduct animal experimentation and the ethical standards of IBIS Ethical Committee. The study was also approved by CNA Scientific Committee. Anaesthetized animals were positioned in the imaging chamber of the microPET scanner (MicroPET Mosaic, Phillips, USA), which was kept at 38°C throughout the experiment. To these mice, 30-37 MBq (0.8 - 1 mCi) of [18F]Amylovis was administered via lateral tail vein injection. The PET data from the 120 min dynamic scans were sorted into three-dimensional sinograms according to the following frame sequence: 10x2 min, 5x5 min and 5x15 min. CT-scans were performed in a NanoScan CT (Mediso, Hungary) at 45 kVp, 240 projections with 500 ms exposition time for anatomical reference. Decay corrected PET images of uniform 1 mm resolution were fused with CT images of uniform 0.2 mm resolution using PMOD 3.3 software (PMOD Technologies Ltd, Switzerland) by a rigid matching method. Then, CT image of the skull was fused in the same software with a predefined mouse brain template acquired in T2-weighted MRI included in PMOD [17], to strip of the skull. The latter transformation was saved and applied to microPET images. This way, fused PET/CT images of 0.2 mm uniform resolution were obtained. Regions of interest were predefined in the template including: cerebellum, cortex, hypothalamus, thalamus, hippocampus, basal ganglia and brain stem. Radiopharmaceutical uptake was also evaluated in bladder, heart, liver, spleen, kidney, muscle and bone by means of PET images.

2.5.3. Immunohistochemical Study

Once the imaging study was concluded, deeply anaesthetized animals were perfused with a solution of 4% paraformaldehyde in 0.01 mol/L PBS pH=7.2. After death, their brains were removed, washed with saline, dried out, both hemispheres were separated and included in paraffin. Then, brains were sectioned in 4 µm thickness slices using a microtome. The sections were deparaffinized, hydrated in

distilled water and treated with 70% formic acid for 30 min to retrieve the antigens. Afterwards, the slices were treated with 3% H_2O_2 for 30 min, to remove residual peroxidase activity, and rinsed again with 0.01 mol/L PBS pH=7.2. Sections were then incubated overnight at 4°C with an anti-Aβ_{1-42} monoclonal antibody (SIGMA, USA) diluted 1:1000. Then, slices were rinsed with 0.01 mol/L PBS pH=7.2 and incubated firstly with a ready to use secondary antibody (SIGMA, USA) for 30 min and secondly with a ready to use avidin-biotin-complex (SIGMA, USA) for 30 min at room temperature. For the staining, it was employed diamino-benzidine for 10 min. The slices were contrasted with Harris' haematoxylin and mounted in an aqueous medium. Slices from brains of healthy mice were taken as negative controls and received the same treatment showing no specific staining. The images of cortex, hippocampus, striatum, thalamus and cerebellum were visualized with the camera of the microscope Olympus BX51 (Japan).

2.6. Statistics

All numerical data are presented as mean value ± standard deviation. Grubbs' test was employed for outliers. Student's t-test was used to compare the uptake of [18F]Amylovis in brain regions of healthy and AD transgenic mice. A significance level of α=0.05 was considered for all tests.

3. RESULTS AND DISCUSSIONS

3.1. Chemistry

The synthesis of 2-(3-fluoropropyl)-6-methoxy naphthalene derivative [28] was carried out by means of several steps (Scheme **1**).

The first step in this procedure is the bromination of 2-naphthol. This occurs according to the method reported by Koelsch [29] and Reddy [18] with a yield of over 95%. The *O*-alkylation reaction of **1** to afford 2-methoxy-6-bromonaphathalene (**2**) took place with $(CH_3)_2SO_4$ as an alkylating agent, and Cs_2CO_3 as a base [30], in anhydrous acetone with an excellent yield.

The metal-catalyzed cross-coupling reactions (CCR) are carried out between an organometallic compound and an organic halide or *pseudo* halide. Further, it is catalyzed by transition metals, mainly nickel and palladium and recently by iron as a simple catalyst system ($FeCl_3$ or $Fe(acac)_3$) [31-35], due to its low prices and ecological advantages [36-39]. In this reaction sometimes, not only the desired product is obtained but also occurs the formation of impurities due to homo-coupling and β-elimination reactions [31, 32, 40-44]. For this reason, the experimental conditions should be properly controlled [37, 42, 45]. In this work, the CCR were assayed to obtain 3-(6-methoxy-2-naphthyl)propyl-4-methyl-benzenesulfonate (**4**) using $Fe(acac)_3$ or $(FeCl_3)_2$ $(TMEDA)_3$ as catalysts and *N,N,N',N'*-tetramethylethylenediamine (TMEDA) and/or hexamethylenetetramine (HMTA) as coligands [34]. The 1,3-propanediol-*p*-ditosylate (di-Ts), which is a bifunctional molecule, was employed in a molar ratio of 1:0.75 with respect to Grignard reagent (bromo(6-methoxy-2-naphthyl)magnesium, **3**), to avoid the di-substituted product formation (Table **1**).
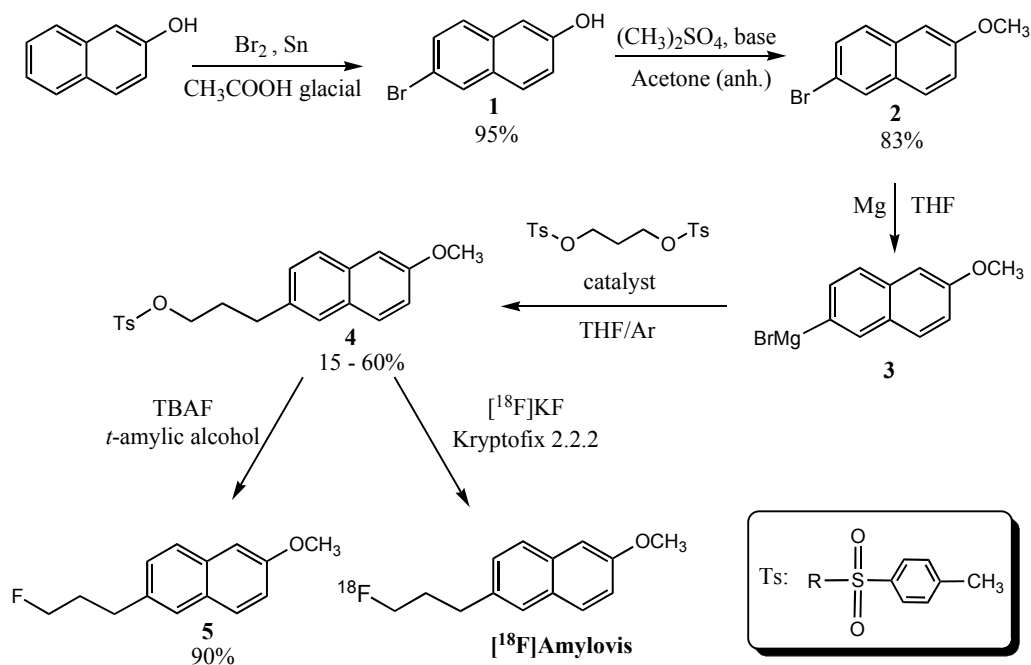
Scheme 1. General procedure for the synthesis of 2-(3-fluoropropyl)-6-methoxynaphthalene (**5**) and [¹⁸F]Amylovis. All reported yields correspond to purified products.

Table 1.   Experimental conditions of the cross-coupling reaction between Grignard reagent (3) and 1,3-dipropanediol-p-ditosylate, at molar ratio 1:0.75, in the presence or not of iron catalyst and coligand, to obtain 3-(6-methoxy-2-naphthyl) propyl 4-methylbenzenesulfonate (4).
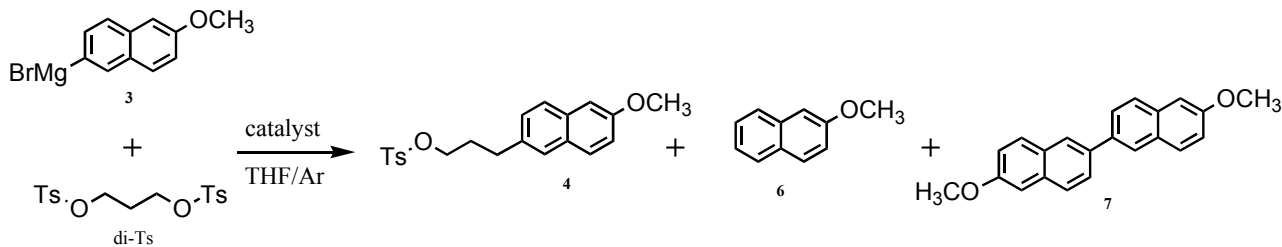
Entry	Catalyst	T (°C)[a]	% Conversion[b]		
			4	**6**	**7**
1	None	-10, 0, 25	-	>90	-
2	(FeCl₃)₂(TMEDA)₃	30[c]	20	70	10
3	(FeCl₃)₂(TMEDA)₃	40[c]	15	65	20
4	(FeCl₃)₂(TMEDA)₃ Coligand: TMEDA (1:1)	70[c]	40	40	20
5	Fe(acac)₃ 5% mol. Coligand 10%: TMEDA, 5% HMTA	0	30	50	20
6	Fe(acac)₃ 5%. Coligand: TMEDA (1:1)	25	60	30	10

[a] Reaction temperature reached after Grignard reagent´s addition. [b] Qualitatively determined by TLC. [c] The Grignard reagent was added at -20 ºC (entries 1 and 2) and 50 ºC (entries 3 and 4).

As it was expected in the absence of a catalyst, the desired product was not achieved even for different reaction temperatures assayed (three independent assays). In the cases that (FeCl₃)₂(TMEDA)₃ was used as a catalyst and Grignard reagent was added at -20°C and 50°C (in Table **1**, entries 2 and 3), the reaction took place unsatisfactorily (low to moderate conversion). When TMEDA was used as a coligand (entry 4), the conversion grade from Grignard reagent to **4** increased up to 40%. Cahiez *et al*. described the use of Fe(acac)₃ and additives (such as TMEDA/HMTA) for CCR, with reaction yields around 70% [34]. Nonetheless, when Fe(acac)₃ and TMEDA/HMTA [34] were employed in CCR (entry 5), the yield was low. The use of TMEDA in a stoichiometric molar ratio or greater with respect to the Grignard reagent is recommended [46] to obtain better yields of product. Thus, similar experimental conditions were assayed (entry 6) and as expected, the conversion grade was higher.

The chemical structure of **4** was confirmed by ¹H- and ¹³C-NMR spectra and mass spectrometry (see Supplementary Material, Fig. (**1S**) to (**5S**)). On the other hand, in the CCR

two by-products were also obtained (Table **1**): 2-methoxynaphthalene (**6**) and 6,6'-dimethyl-2, 2'-binaphthalene (**7**), which were identified by NMR (see Supplementary Material, Fig. (**6S**) to Fig. (**7S**) and Fig. (**8S**) to Fig. (**9S**), respectively).

The nucleophilic fluorination of **4** (Scheme **1**) to obtain 2-(3-fluoropropyl)-6-methoxynaphthalene (**5**) was carried out with tetrabutylammonium fluoride salt (TBAF) and *tert*-amylic alcohol, according to the conditions described by Kim *et al*. [47]. The yield of the reaction was over 90%. The compound was purified by column chromatography and its purity was above 97%, determined by HPLC (see Supplementary Material, Fig. (**10S**)).

The compound **5** was characterized by ^{1}H-, ^{13}C- and 2D NMR techniques (HSQC, HMBC and H-HCOSY) and MS spectrum. In the ^{1}H-NMR spectrum, all protons of the molecule were observed. A doublet of triplets was observed at 4.55 and 4.43 ppm, which was assigned to the methylene group bound to a fluorine atom, with coupling constant ^{2}J of 47.24 Hz. Triplet and multiplet signals observed at 2.88 and 2.17-2.04 (^{3}J= 26.15 Hz) ppm, corresponded to the methylene groups bound to naphthyl ring and to the internal of the alkylic chain, respectively (see Supplementary Material, Fig. (**11S**). The ^{13}C-NMR spectrum confirmed the structure of **5** and methylene groups were observed, as doublets, with the following coupling constants: ^{1}J$_{C-F}$ = 164.30, ^{2}J$_{CC-F}$ = 19.76 and ^{3}J$_{CCC-F}$ = 5.86 Hz (see Supplementary Material, Fig. (**12S**). Finally, in the TOF-ESI-MS the molecular ion peak at m/z 219.14 (around 75% abundance) was detected, confirming the structure of **5** (see Supplementary Material, Fig. (**13S**)).

3.2. *In silico* Studies

Aβ$_{1-42}$ peptide and its conformational changes have been used as a molecular target for docking and molecular dynamics simulations to find compounds that can be employed as imaging probes for AD diagnosis or treatment [48-50]. It is known that there are three natural steric zippers due to the polymorphism of this peptide, which plays a key role in the β-cross structure formation. In the Aβ$_{1-42}$ peptide, the most studied steric zipper is located in the region from 16 to 21 a.a. (KLVFFA) [51-53]. In this work, a combination of docking and dynamic simulations along with binding free energy calculations (by Linear Interaction Energy, LIE) were done in order to understand the affinity and temporal stability of the complexes: 2-(3-fluoropropyl)-6-methoxynaphthalene (**5**)-Aβ peptide and PIB-Aβ peptide.

According to the rigid docking simulation, **5** interacts with amino acids 4-25 of Aβ peptide in all simulations, mainly with residues F4, D7, Y10, E11 Q15 K16 V18 F19 and F20. Under similar simulation conditions, PIB interacts with the amino acids 7-20 of Aβ peptide (in all simulations), mainly with residues D7 S8 E11 V12 Q15 K16 and F19 (see Supplementary Material, Fig. (**14S**)).

A flexible docking approach was used, wherein all amino acids in this binding site were selected to have flexible side chains during simulation (Fig. **1**).

In the 99% of calculations for **5**, the interaction zone included amino acids from 12 to 21, specifically with the residues Q15, K16, V18, F19, F20 (RMSD < 2 Å). In general, **5**

binds to these residues via hydrophobic interactions and Van der Waals forces. The π-π interactions were located between the naphthyl ring of the ligand and the phenyl ring of the F19 and F20 residues, mainly with F19 (Fig. **1A**). Similar amino acids are involved in the interaction between PIB and peptide (RMSD < 2 Å) (Fig. **1B**). In this case, it was found an H-bond between the nitrogen atom of the benzothiazole ring of PIB and the hydrogen atom of amine group of K16, also a π-π hydrophobic interaction was located between the phenyl rings of PIB and F19.

A

DAEFRHDSGYE**V**HH**QK**L**VFF**AEDVG**S**NKGAIIGLMVGGVVIA

B

DAEFRH**DS**GY**EV**HH**QK**L**VF**FAEDVG**S**NKGAIIGLMVGGVVIA
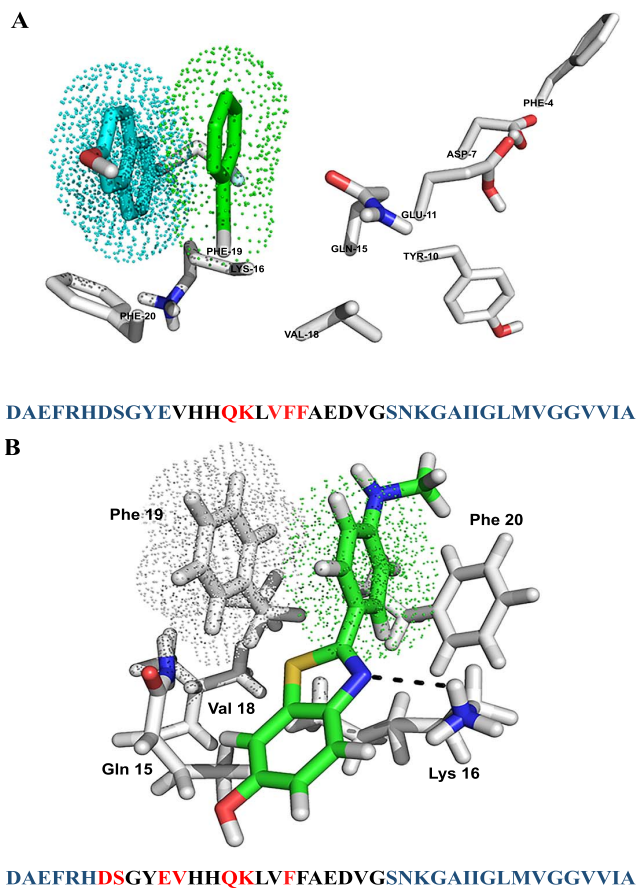
Fig. (1). A: Flexible docking of **5** (at 5 Å distance): the π-π hydrophobic interactions were located between the naphthyl ring of **5** and the phenyl ring of the F19 and F20 residues. **B**: Flexible docking of PIB (at 5 Å distance): the H-bond was located between nitrogen atom of the benzothiazole ring of PIB and hydrogen atom of -NH$_2$ group of K16, and also a π-π hydrophobic interaction was located between the phenyl rings of PIB and F19.

The molecular dynamics (MD) calculations provide more detailed information about the stability of the ligand-peptide complex into biological environment, along the time. Two different assays were carried out: a) when the ligand **5** is near to Aβ$_{1-42}$ peptide (< 4 Å) (MD study I (see Supplementary Material, Fig. (**15S**); and b) when the ligands are transferred outside of the peptide interaction field (10 Å) (MD study II, Fig. **2**).

In MD studies (I and II), **5** interacts with the Aβ$_{1-42}$ peptide in the same region defined in dockings simulations. The calculated RMSD values were less to 2 Å during the assayed times which indicates that the interaction zone was practically unchanged. A similar result was obtained in MD study

A

Initial time - 0 ns   15 ns   30 ns

B

C
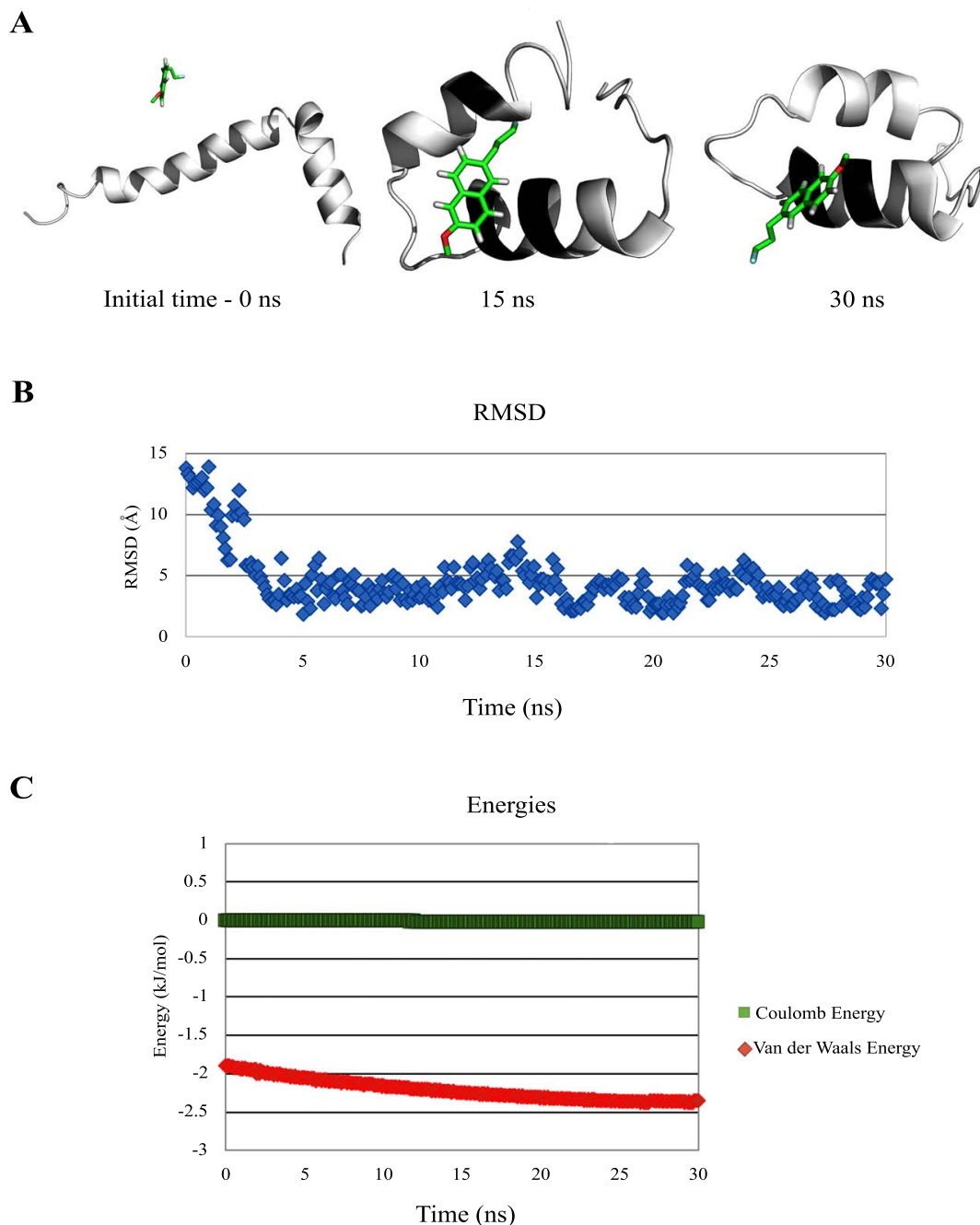
Fig. (2). Molecular Dynamics (MD) study II of 2-(3-fluoropropyl)-6-methoxynaphthalene (**5**). **A**: Evolution of different conformations of the ligand-Aβ$_{1-42}$ peptide complex (at 10 Å) during different times. **B**: Root Mean Square Deviation (RMSD) of **5** position with respect to the Aβ peptide. **C**: Van der Waals (red) and electrostatic (green) energies for ligand-Aβ peptide complex at each time interval during MD simulations.

II for PIB-Aβ peptide complex (see Supplementary Material, Fig. (**16S**)).

The calculation of the free energy (ΔG) was carried out using the LIE method for free energy. This method uses an average of the interactions between the ligand and its environment obtained by MD studies. The values of the mean square deviation errors, compared to the experimental energies, are less than ~ 1 kcal/mol [27, 54]. The ΔG values for **5**-Aβ peptide complex indicated that at the beginning of the simulation there was no contact between the Aβ peptide and **5**, therefore ΔG values were positives. After 5 ns of calcula-

tion, the ligand-peptide complex became more stable, with an average ΔG value of -5.31 kcal/mol. Similar behavior was obtained for PIB-Aβ peptide complex and the ΔG value was -4.12 kcal/mol.

3.3. Radiosynthesis

The radiosynthesis of compound 2-(3-[¹⁸F]fluoropropyl)-6-methoxynaphthalene ([¹⁸F]Amylovis) was carried out in an automated synthesis platform. The labelled compound was purified by semi-preparative HPLC, and solid phase extraction (SPE) (Fig. **3**). [¹⁸F]Amylovis was obtained with a ra-

diochemical purity of 99.3% ± 0.3 (n=3). In all cases, the difference between retention times of [^{18}F]Amylovis and **5** was below 4%, as shown in Fig. (**3**). Radionuclide identity and purity were confirmed by measuring its half-life and gamma spectrum, in all the batches. The global yield of synthesis was 24 ± 1% (decay corrected) and the specific activity was 351-616 GBq/µmol (see Supplementary Material, Table **1S** and Fig. (**17S**)).

The log $P_{oct/PBS}$ value of [^{18}F]Amylovis was 2.46 ± 0.06 (two independent experiments, in triplicate), indicating that this radiopharmaceutical is moderately lipophilic (see Supplementary Material, Table **2S**), allowing to predict its ability to passively cross the BBB.

3.4. *In vitro* Stability Studies

The *in vitro* stability assay (radiochemical purity) of the final formulation of [^{18}F]Amylovis showed that the compound did not significantly change after 6 h, at room temperature (see Supplementary Material, Table **3S**). In addi-

tion, the radiotracer was not degraded in fresh human plasma after 2 h incubation at 37ºC (see Supplementary Material, Table **4S**). Plasma protein binding (PPB) determination was carried out by gel filtration. The product showed a high PPB percentage, which was constant over time (see Supplementary Material, Table **5S**).

3.5. The Binding Affinity Constants of [^{18}F]Amylovis and [^{11}C]PIB

The *in vitro* affinity assessment of [^{18}F]Amylovis and [^{11}C]PIB to Aβ plaques was performed on brain serial sections from homozygous B6; 129-Psen1^{tm1Mpm}Tg(APPSwe,tau P301L)1Lfa/Mmjax mice (3xTg-AD, 9 months, female), by means of saturation and competitive binding assays. This strain of transgenic mice exhibits Aβ plaques and tangles associated with synaptic dysfunction, traits similar to those observed in AD patient brains. According to [55, 56], Aβ plaques have been detected in some brain regions since 3-4 months and deficits in the cognition have at 6 months. The binding affinity constants calculated for [^{18}F]Amylovis and
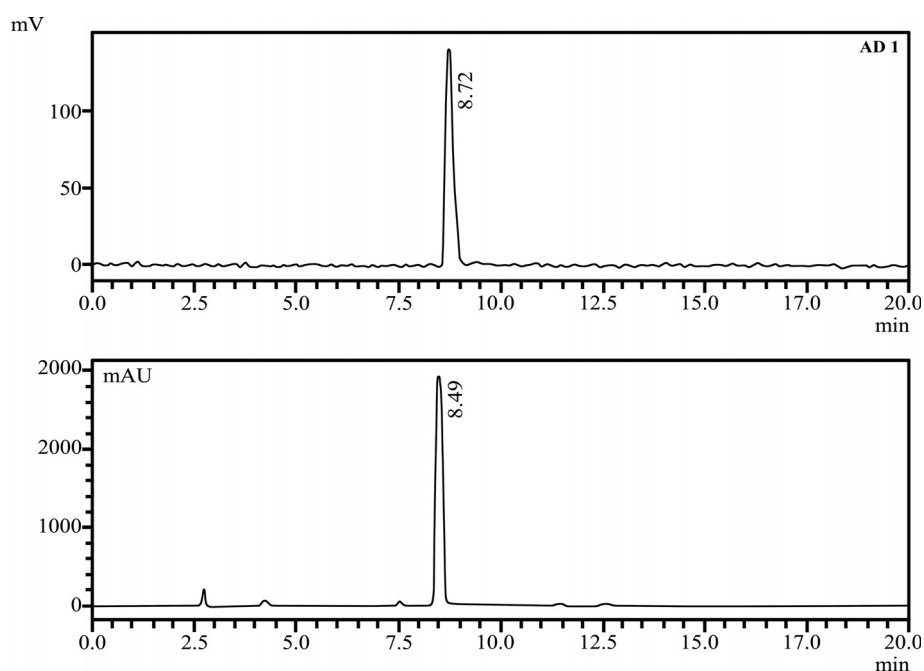
Fig. (3). HPLC chromatograms of **5** (**A**) and [^{18}F]Amylovis (**B**) after purification with C18 light-SPE cartridge, retention times: 8.5 and 8.7 min, respectively, and a purity > 99% for both compounds. Chromatographic conditions: Phenomenex Luna C18 (250 x 4.6 mm, 5 µm) column; mobile phase: AcN:H$_2$O (75:25); flow rate: 1 mL/min.

Table 2. Lipophilicity (log P) and Aβ binding affinity (K_d) of [^{18}F]Amylovis, [^{11}C]PIB and others Aβ imaging probes.

Compounds	K_d (nM)	Log P	Amyloid Sample
[^{18}F]Amylovis	0.16	2.46 ± 0.06[a]	Brain serial sections of 3xTg-AD mice
[^{11}C]PIB	8.86	1.3 [61]	Brain serial sections of 3xTg-AD mice
[^{11}C]PIB	2.5 [58]	1.3 [61]	AD brain homogenates
[^{18}F]Florbetapir, AV-45	3.72 [62]	2.4 [63]	AD brain homogenates
[^{18}F]Flutemetamol, GE-067	6.7 [59]	1.7 [64]	AD brain homogenates
[^{18}F]Florbetaben, BAY94-9172	16 [60]	2.41 [65]	AD brain homogenates

[a] log P values determined by octanol-buffer partitioning.

[^{11}C]PIB, and their Lop P values are shown in Table **2**, along with other Aβ imaging probes [57-60].

According to our results, [^{18}F]Amylovis and [^{11}C]PIB displayed a saturable binding and its data transformation to Scatchard plots showed a binding [65] fitted to a single binding site with a good correlation, having a K_d of 0.16 nM (r > 0.96) and 8.86 nM (r > 0.88), respectively, indicating a specific binding. [^{18}F]Amylovis showed 6-fold higher affinity for Aβ plaques compared with [^{11}C]PIB, whereas the concentration of potential Aβ binding sites was 16-fold higher for [^{11}C]PIB (B_{max} = 1967 nM) than for [^{18}F]Amylovis (B_{max} = 119.4 nM). One of the main requirement for designing optimal brain-radiotracer is the binding potential (BP; ratio of Bmax/K_d) which should be higher than 10 [66]. BP value of [^{18}F]Amylovis is 741, 3-folds higher than the [^{11}C]PIB (BP = 222), in the evaluated conditions, indicating that [^{18}F]Amylovis has excellent affinity for Aβ plaques in the brain section of homozygous 3xTg-AD mice (see Supplementary Material, Fig. (**18S**) and Fig. (**19S**)).

3.6. Biodistribution Study

Biodistribution of [^{18}F]Amylovis in healthy Balb/C male mice, at different times after i.v. the administration is summarized in Fig. (**4**).

The high uptake values of [^{18}F]Amylovis in kidneys and liver suggest that the urinary and hepatobiliary tracts were the main elimination pathways of this radiotracer; whilst the %ID/g (percentage injected dose per gram tissue) in kidneys was higher than values reported for other compounds with

similarly estimated liposolubility [66]. The uptake peak of [^{18}F]Amylovis in the brain of healthy Balb/c mice (around 7% ID/g at the starting biodistribution point) and its fast clearance (0.11±0.03 %ID/g at 60 min), indicate that this radiotracer passive efficiently cross the normal BBB like other PET radiopharmaceuticals directed against Aβ plaque [57, 67]. The relatively high bone uptake suggests a possible *in vivo* defluorination, but this is more prevalent in rodents than in primates [68]. Nevertheless, it is known that free fluorine should not be taken up by the brain; therefore, it should not interfere with the imaging of this tissue. Plasma clearance ($T_{1/2}$ = 37±10 min) is comparable to the reported estimated half-life of [^{18}F]Florbetaben [57], considering that [^{18}F]Amylovis is estimated to be a more lipophilic compound. The high values of volume of distribution at steady state (Vss, 10.3 ± 2.9 mL) and Vss/kg (372 ± 110 mL/kg) indicate that [^{18}F]Amylovis is deeply internalized, available to cross BBB and to reach the brain tissue (see Supplementary Material, Table **6S**).

3.7. MicroPET/CT Images Dynamic Images of [^{18}F]Amylovis

The APPswe/PS1dE9 transgenic mouse model used in our study overexpresses the Swedish mutation of APP, together with PS1 deleted in exon 9 each driven by mouse PrP promoter. These mice develop the first plaques at four months of age, mainly in cortical areas and hippocampus [27]. Dynamic images of [^{18}F]Amylovis in brain tissue revealed a significant difference between the kinetic uptake in control healthy (C57BL/6, wild) and in transgenic mice. The uptake of
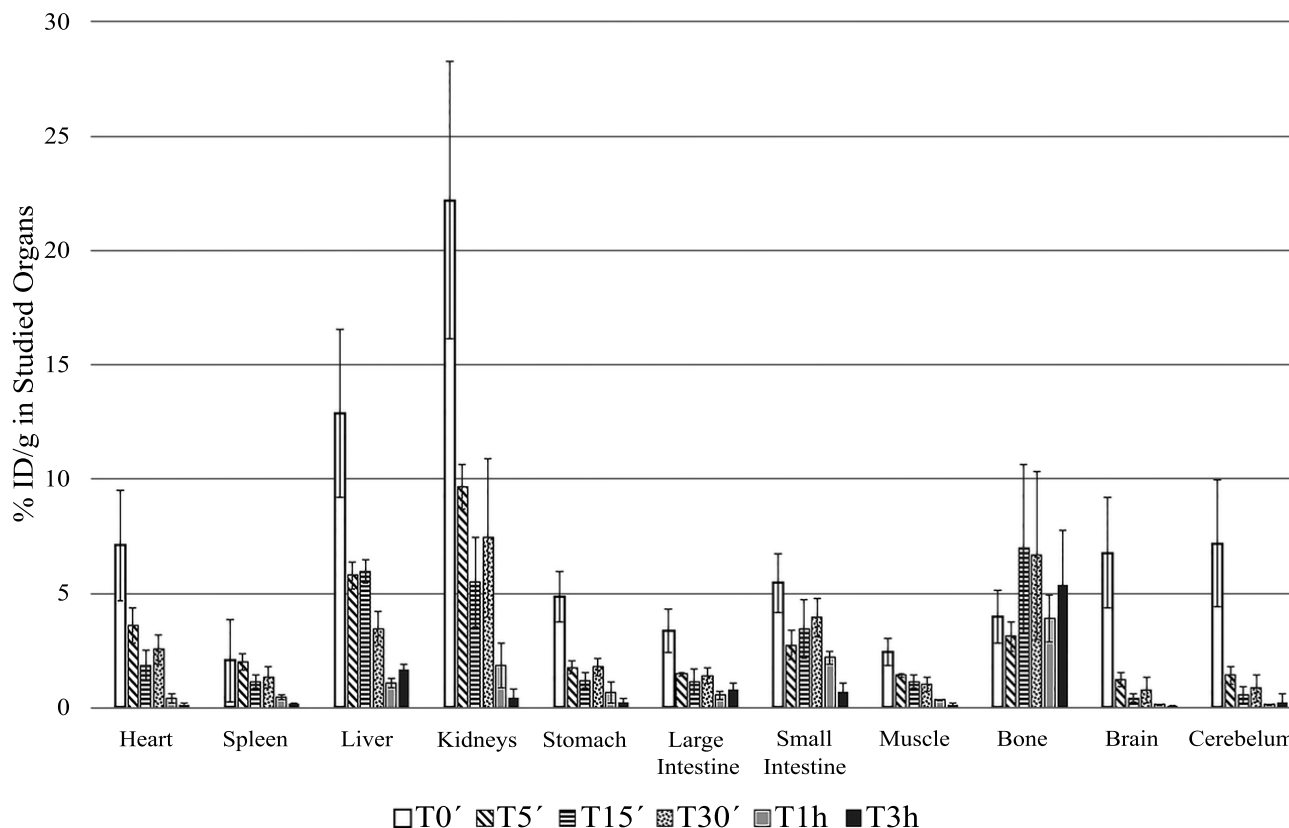
Fig. (4). Biodistribution of [^{18}F]Amylovis in healthy Balb/C male mice (10-12 week-old and 28.5±2.0 g). %ID/g (percentage injected dose per gram tissue).

[18F]Amylovis in the cortex at different time intervals in control healthy and APPSwe/PS1dE9 mice is shown in Fig. (**5**).

Similarly, wild-type mice showed maximum activity at 2 min with a fast washout, in accordance with the results of biodistribution study; however, transgenic mice had slower uptake kinetics, with a peak at 23-25 min and a less pronounced washout. Such differences could be related to the specific binding of the tracer for the plaques in brain. Further studies should be conducted in order to have more evidence of this issue, as reported for other radiotracers by other authors [66].

Considering that maximal cortex uptake of the [18F]Amylovis was observed in dynamic images at about 25 min after administration, static PET images were performed at 30 min. Brendel M. *et al.* [2] found that the presence of amyloid plaques in cerebellar tissue of APPswe/PS1dE9 mice can significantly affect the standardized uptake value (SUV) relative to the cerebellum. Therefore, in the analysis of static images, the SUV was normalized at brain stem as proposed by other authors [2, 8].

Comparative SUV of [18F]Amylovis in some brain regions, regarding the brain stem, is summarized in Fig. (**6**) (n=3).
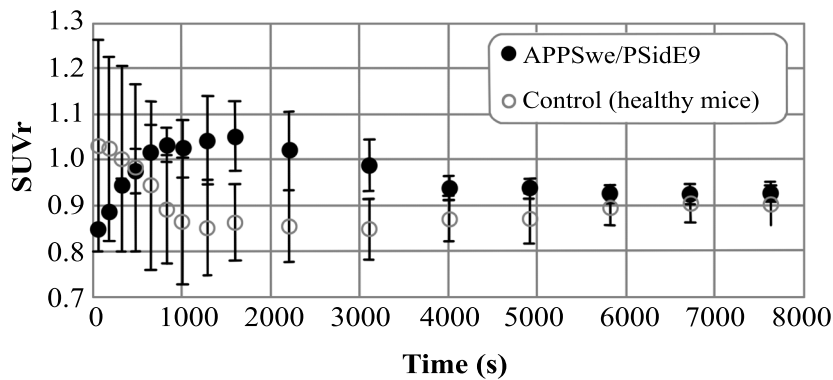
Fig. (5). Comparative standardized uptake value relative (SUVr) curves (cortex/cerebellum) of [18F]Amylovis in healthy (control) vs APPSwe/PS1dE9 mice up to 130 min. Each point represents mean values ± standard deviation (n=4).
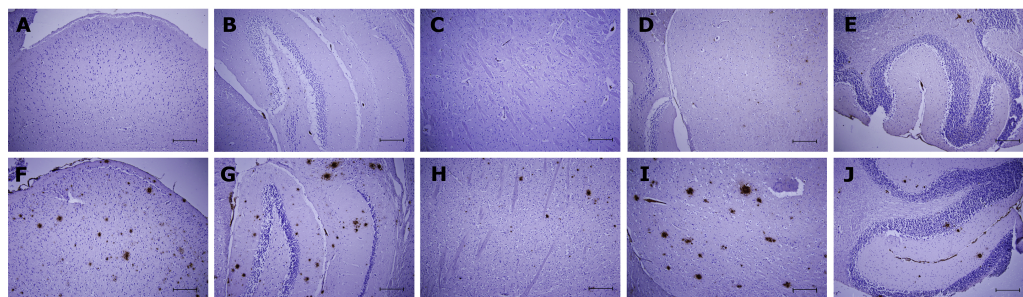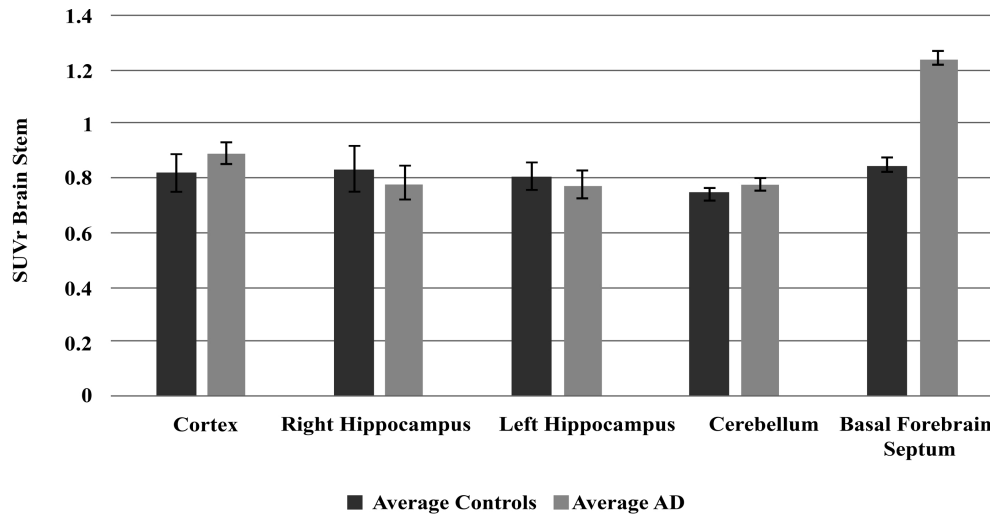
Fig. (6). I. Comparison of standardized uptake values in regard to the brain stem, SUVr, of [18F]Amylovis in some brain regions between control healthy and APPSwe/PS1dE9 mice (n=3). **II**. Representative microphotograph of the prefrontal cortex (**A**, **F**), hippocampus (**B**, **G**), striatum (**C**, **H**), thalamus (**D**, **I**) and cerebellum (**E**, **J**). Set of images A-E corresponds to healthy animals and F-J to transgenic APPSwe/PS1dE9 mice (scale bar = 400 μm).

According to the immunohistochemical study, we found a significant number of amyloid plaques in the analyzed brain areas of APPSwe/PS1dE9 mice (Fig. **6-II**) and among the cortex, hippocampus and thalamus presented the highest values, while cortex significantly differed from striatum and cerebellum (Duncan's test, $F_{(4,100)}$ = 4.98, p=0.001). Meanwhile, brain slices of control healthy mice showed an absence of β-amyloid deposits. A significantly augmented uptake of [^{18}F]Amylovis was observed in basal forebrain septum of transgenic animals in comparison to control healthy mice (p=0.0025) and a slightly incremented uptake of the radiopharmaceutical in cortex of transgenic mice was also found, despite it had no statistical significance. This fact could be influenced by the small size of the sample and also the age of transgenic mice (12 months). An incremented number of amyloid plaques in APPSwe/PS1dE9 mice in regard to control healthy C57BL/6 mice was confirmed by the immunohistochemical assay.

CONCLUSION

2-(3-fluoropropyl)-6-methoxynaphthalene was successfully synthesized through an efficient procedure, that involves a cross-coupling reaction with a Grignard reagent and 1,3-dipropanediol-*p*-ditosylate as an electrophilic agent. The "cold" fluorinated compound 2-(3-fluoropropyl)-6-methoxynaphthalene was achieved with a high yield, using tetrabutylammonium fluoride salt in *tert*-amylic alcohol. *In silico* simulations indicated that 2-(3-fluoropropyl)-6-methoxynaphthalene forms a stable complex with the β-amyloid peptide by hydrophobic interactions, specifically with the amino acids Q15, K16, V18, F19, F20. This region was identified as a steric zipper implicated in the β-cross structure of Aβ plaques. The precursor, 3-(6-methoxy-2-naphthyl)propyl-4-methyl benzenesulfonate, was radiolabeled with [^{18}F]fluoride with a satisfactory yield (24.2 ± 1.4%), high radiochemical purity (> 99%) and specific activity (from 351 to 616 GBq/μmol). The log $P_{oct/PBS}$ value of [^{18}F]Amylovis point out to mild lipophilicity. Results of the *in vitro* binding assays in *postmortem* brain serial sections of 3xTg-AD mice showed an effective binding profile for the detection of Aβ plaques, which is in accordance with the outcomes of the *in silico* studies. In the biodistribution assay using healthy mice, [^{18}F]Amylovis shows good uptake into (7 %ID/g at 5 min post-injection) and fast clearance (0.11±0.03 %ID/g at 60 min) from the brain, which reveals that it passively cross the normal BBB. The kinetic uptake of [^{18}F]Amylovis in brain tissue of control healthy and transgenic mice is significantly different and the immunohistochemical study is in accordance with this results. All these results suggest that this compound could be a new potential PET probe for *in vivo* detection Aβ plaques in AD brains. Nevertheless, further studies should be accomplished to complete its preclinical assessment.

ETHICS APPROVAL AND CONSENT TO PARTICIPATE

The study was approved by the Ethics Committee of Universidad de Sevilla (*Dirección General de la Producción Agrícola y Ganadera*), Sevilla, Spain (Reference Number: 25-10-2016-168).

HUMAN AND ANIMAL RIGHTS

No humans were involved in this study. The reported experiments on animals were in accordance with the standards set of the Guide for the Care and Use of Laboratory Animals of the *Dirección General de la Producción Agrícola y Ganadera (artículo 34 del RD 53/2013 de 1 de Febrero. (Consejería de Medio Ambiente, Administración Local y Ordenación del Territorio-Comunidad de Madrid)*.

CONSENT FOR PUBLICATION

Not applicable.

CONFLICT OF INTEREST

The authors declare no conflict of interest, financial or otherwise.

SUPPLEMENTARY MATERIAL

Supplementary material is available on the publisher's website along with the published article.

REFERENCES

[1]   Selkoe, D.J.; Hardy, J. The amyloid hypothesis of Alzheimer's disease at 25 years. *EMBO Mol. Med.,* **2016**, *8*(6), 595-608.

[2]   Sperling, R.A.; Aisen, P.S.; Beckett, L.A.; Bennett, D.A.; Craft, S.; Fagan, A.M.; Iwatsubo, T.; Jack, C.R.; Kaye, J.; Montine, T.J. Toward defining the preclinical stages of Alzheimer's disease: Recommendations from the National Institute on Aging-Alzheimer's Association workgroups on diagnostic guidelines for Alzheimer's disease. *Alzheimers Dement.,* **2011**, *7*(3), 280-292.

[3]   Scheuner, D.; Eckman, C.; Jensen, M.; Song, X.; Citron, M.; Suzuki, N.; Bird, T.; Hardy, J.; Hutton, M.; Kukull, W. Secreted amyloid β-protein similar to that in the senile plaques of Alzheimer's disease is increased *in vivo* by the presenilin 1 and 2 and APP mutations linked to familial Alzheimer's disease. *Nat. Med.,* **1996**, *2*(8), 864-870.

[4]   Monsonego, A.; Weiner, H.L. Immunotherapeutic approaches to Alzheimer's disease. *Science,* **2003**, *302*(5646), 834-838.

[5]   DeKosky, S.T.; Marek, K. Looking backward to move forward: Early detection of neurodegenerative disorders. *Science,* **2003**, *302* (5646), 830-834.

[6]   Prince, M.; Wimo, A.; Guerchet, M.; Ali, G.; Wu, Y.; Prina, M. World Alzheimer Report 2015. The global impact of dementia. An analysis of prevalence, incidence, cost and trends. *Alzheimer's Disease International, London,* **2015**. https://www.alz.co.uk/research/world-report-2015.

[7]   Salerno, M.; Porqueras, D.S.D. Alzheimer's disease: The use of contrast agents for magnetic resonance imaging to detect amyloid beta peptide inside the brain. *Coord. Chem. Rev.,* **2016**, *327*, 27-34.

[8]   Anthony, M.; Lin, F. A systematic review for functional neuroimaging studies of cognitive reserve across the cognitive aging spectrum. *Arch Clin Neuropsychol.,* **2018**, *33*(8), 937-948.

[9]   Yang, Y.; Zhang, X.; Cui, M.; Zhang, J.; Guo, Z.; Li, Y.; Zhang, X.; Dai, J.; Liu, B. Preliminary characterization and *in vivo* studies of structurally identical 18 f-and 125 i-labeled benzyloxybenzenes for PET/SPECT imaging of β-amyloid plaques. *Sci. Rep.,* **2015**, *5*, 12084.

[10]   Morris, E.; Chalkidou, A.; Hammers, A.; Peacock, J.; Summers, J.; Keevil, S. Diagnostic accuracy of 18 F amyloid PET tracers for the diagnosis of Alzheimer's disease: A systematic review and meta-analysis. *Eur. J. Nucl. Med. Mol. Imaging,* **2016**, *43*(2), 374-385.

[11]   Catafau, A.M.; Bullich, S. Amyloid PET imaging: Applications beyond Alzheimer's disease. *Clin. Transl. Imaging,* **2015**, *3*(1), 39-55.

[12]   Furumoto, S.; Okamura, N.; Iwata, R.; Yanai, K.; Arai, H.; Kudo, Y. Recent advances in the development of amyloid imaging agents. *Curr. Top. Med. Chem.,* **2007**, *7* (18), 1773-1789.

[13]   Kung, H.F.; Choi, S.R.; Qu, W.; Zhang, W.; Skovronsky, D. 18F stilbenes and styrylpyridines for PET imaging of A beta plaques in Alzheimer's disease: A miniperspective. *J. Med. Chem.,* **2010**, *53*(3), 933-941.

[14]   Choi, S.R.; Schneider, J.A.; Bennett, D.A.; Beach, T.G.; Bedell, B.J.; Zehntner, S.P.; Krautkramer, M.; Kung, H.F.; Skovronsky, D.M.; Hefti, F. Correlation of amyloid PET ligand florbetapir F 18 (18F-AV-45) binding with β-amyloid aggregation and neuritic plaque deposition in postmortem brain tissue. *Alzheimer Dis. Assoc. Disord.,* **2012**, *26*(1), 8-16.

[15]   de Lartigue, J. Flutemetamol (18F): A β-amyloid positron emission tomography tracer for Alzheimer's and dementia diagnosis. *Drugs Today,* **2014**, *50* (3), 219-229.

[16]   Villemagne, V.L.; Ong, K.; Mulligan, R.S.; Holl, G.; Pejoska, S.; Jones, G.; O'Keefe, G.; Ackerman, U.; Tochon-Danguy, H.; Chan, J.G. Amyloid imaging with 18F-florbetaben in Alzheimer disease and other dementias. *J. Nucl. Med.,* **2011**, *52*(8), 1210-1217.

[17]   Ma, Y.; Hof, P.R.; Grant, S.C.; Blackband, S.J.; Bennett, R.; Slatest, L.; McGuigan, M.D.; Benveniste, H. A three-dimensional digital atlas database of the adult C57BL/6J mouse brain by magnetic resonance microscopy. *Neuroscience,* **2005**, *135*(4), 1203-1215.

[18]   Prabhakar, C.; Reddy, G.B.; Reddy, C.M.; Nageshwar, D.; Devi, A.S.; Babu, J.M.; Vyas, K.; Sarma, M.; Reddy, G.O. Process research and structural studies on nabumetone. *Org. Process Res. Dev.,* **1999**, *3*(2), 121-125.

[19]   Berman, H.M.; Westbrook, J.; Feng, Z.; Gilliland, G.; Bhat, T.N.; Weissig, H.; Shindyalov, I.N.; Bourne, P.E. *The Protein Data Bank, 1999-*. Springer, Dordrecht: 2006.

[20]   Hanwell, M.D.; Curtis, D.E.; Lonie, D.C.; Vandermeersch, T.; Zurek, E.; Hutchison, G.R. Avogadro: An advanced semantic chemical editor, visualization, and analysis platform. *J. Cheminf.,* **2012**, *4*(1), 17.

[21]   Trott, O.; Olson, A.J. AutoDock Vina: Improving the speed and accuracy of docking with a new scoring function, efficient optimization, and multithreading. *J. Comput. Chem.,* **2010**, *31*(2), 455-461.

[22]   Hess, B.; Kutzner, C.; Van Der Spoel, D.; Lindahl, E. GROMACS 4: Algorithms for highly efficient, load-balanced, and scalable molecular simulation. *J. Chem. Theory Comput.,* **2008**, *4*(3), 435-447.

[23]   Case, D.A.; Cheatham, T.E.; Darden, T.; Gohlke, H.; Luo, R.; Merz, K.M.; Onufriev, A.; Simmerling, C.; Wang, B.; Woods, R.J. The Amber biomolecular simulation programs. *J. Comput. Chem.,* **2005**, *26*(16), 1668-1688.

[24]   Lemkul, J.A.; Allen, W.J.; Bevan, D.R. Practical considerations for building GROMOS-compatible small-molecule topologies. *J. Chem. Inf. Model.,* **2010**, *50*(12), 2221-2235.

[25]   Klunk, W.E.; Wang, Y.; Huang, G.F.; Debnath, M.L.; Holt, D.P.; Mathis, C.A. Uncharged thioflavin-T derivatives bind to amyloid-beta protein with high affinity and readily enter the brain. *Life Sciences,* **2001**, *69* (13), 1471-1484.

[26]   Klunk, W.E.; Wang, Y.; Huang, G.-f.; Debnath, M.L.; Holt, D.P.; Shao, L.; Hamilton, R.L.; Ikonomovic, M.D.; DeKosky, S.T.; Mathis, C.A. The binding of 2-(4′-methylaminophenyl)

[27]   benzothiazole to postmortem brain homogenates is dominated by the amyloid component. *J. Neurosci.,* **2003**, *23*(6), 2086-2092.

[27]   Wang, R.; Lai, L.; Wang, S. Further development and validation of empirical scoring functions for structure-based binding affinity prediction. *J. Comput.-Aided Mol. Des.,* **2002**, *16*(1), 11-26.

[28]   Sablón, M.; Rodriguez, C.; Rivera, S.; Pérez, R.; Perera, A.; López, R.M. Method for obtaining novel derivatives of naphthalene for *in vivo* diagnosis of Alzheimer's disease. *Registered with the Cuban Industrial Property Office, under No. 2009/57 and registration number 23844 in the same office. This patent was granted by: European Patent Office (EPO 2 436 666 A20), Unitted State Patent (US 9,764,047), Instituto Mexicano de la Propiedad industrial (MX/a/2013/011331), Canadian intellectual Property Office (CA2789869 C), South African Patent Office (No. 2012/07005) and Intellectual Property Corporation of Malaysian (PI 2012003534). Also, the patent is requested in US (2012/0321560 A1), Brazil (PI0115172-0) and in Japan (9/2012),* **2009**.

[29]   Koelsch, F.C. 6-Bromo-2-naphthol. *In EC Horning, ed, Organic Synthesis Collective Vol 3, A Revised Edition Of Annual Volumes 20-29. John Wiley & Sons, Inc., New York,* **1995**, 132-133.

[30]   Dijkstra, G.; Kruizinga, W.H.; Kellogg, R.M. An assessment of the causes of the "cesium effect". *J. Org. Chem.,* **1987**, *52*(19), 4230-4234.

[31]   Fü rstner, A.; Martin, R.; Krause, H.; Seidel, G.n.; Goddard, R.; Lehmann, C.W. Preparation, structure, and reactivity of nonstabilized organoiron compounds. Implications for iron-catalyzed cross coupling reactions. *J. Am. Chem. Soc.,* **2008**, *130* (27), 8773-8787.

[32]   Fürstner, A.; Leitner, A. Iron-catalyzed cross-coupling reactions of alkyl-grignard reagents with aryl chlorides, tosylates, and triflates. *Angew. Chem., Int. Ed.,* **2002**, *41*(4), 609-612.

[33]   Fürstner, A.; Leitner, A.; Méndez, M.; Krause, H. Iron-catalyzed cross-coupling reactions. *J. Am. Chem. Soc.,* **2002**, *124*(46), 13856-13863.

[34]   Cahiez, G.; Habiak, V.; Duplais, C.; Moyeux, A. Iron-catalyzed alkylations of aromatic grignard reagents. *Angew. Chem., Int. Ed.,* **2007**, *46*(23), 4364-4366.

[35]   Martin, R.; Fürstner, A. Cross-coupling of alkyl halides with aryl grignard reagents catalyzed by a low-valent iron complex. *Angew. Chem.,* **2004**, *116*(30), 4045-4047.

[36]   Bedford, R.B.; Brenner, P.B. The development of iron catalysts for cross-coupling reactions. In *Iron Catalysis II*, Springer: 2015; pp 19-46.

[37]   Nagano, T.; Hayashi, T. Iron-catalyzed Grignard cross-coupling with alkyl halides possessing β-hydrogens. *Org. Lett.,* **2004**, *6*(8), 1297-1299.

[38]   Tamura, M.; Kochi, J.K. Vinylation of Grignard reagents. Catalysis by iron. *J. Am. Chem. Soc.,* **1971**, *93*(6), 1487-1489.

[39]   Kochi, J.K. Electron-transfer mechanisms for organometallic intermediates in catalytic reactions. *Acc. Chem. Res.,* **1974**, *7*(10), 351-360.

[40]   Yamamoto, A. Organotransition-metal chemistry: Past development and future outlook. *J. Organomet. Chem.,* **2000**, *600* (1), 159-167.

[41]   Uchino, M.; Yamamoto, A.; Ikeda, S. Preparation of a phenyl—nickel complex, phenyl (dipyridyl) nickel chloride, an olefin dimerization catalyst. *J. Organomet. Chem.,* **1970**, *24*(3), C63-C64.

[42]   Nakamura, M.; Matsuo, K.; Ito, S.; Nakamura, E. Iron-catalyzed cross-coupling of primary and secondary alkyl halides with aryl Grignard reagents. *J. Am. Chem. Soc.,* **2004**, *126*(12), 3686-3687.

[43]   Bedford, R.B.; Betham, M.; Bruce, D.W.; Danopoulos, A.A.; Frost, R.M.; Hird, M. Iron− Phosphine,− Phosphite,− Arsine, and-Carbene Catalysts for the Coupling of Primary and Secondary Alkyl Halides with Aryl Grignard Reagents. *J. Org. Chem,* **2006**, *71* (3), 1104-1110.

[44]   Nakamura, M.; Ito, S.; Matsuo, K.; Nakamura, E. Iron-catalyzed chemoselective cross-coupling of primary and secondary alkyl halides with arylzinc reagents. *Synlett,* **2005**, *2005* (11), 1794-1798.

[45]   Karlstroem, A.S.E.; Huerta, F.F.; Meuzelaar, G.J.; Bäckvall, J.-E. Ferrocenyl thiolates as ligands in the enantioselective copper-catalyzed substitution of allylic acetates with Grignard reagents. *Synlett,* **2001**, *2001* (Special Issue), 0923-0926.

[46]   Noda, D.; Sunada, Y.; Hatakeyama, T.; Nakamura, M.; Nagashima, H. Effect of TMEDA on iron-catalyzed coupling reactions of ArMgX with Alkyl halides. *J. Am. Chem. Soc.,* **2009**, *131* (17), 6078-6079.

[47] Kim, D.W.; Jeong, H.-J.; Lim, S.T.; Sohn, M.-H. Facile nucleophilic fluorination of primary alkyl halides using tetrabutylammonium fluoride in a tert-alcohol medium. *Tetrahedron Lett.,* **2010**, *51*(2), 432-434.

[48] Chang, W.E.; Takeda, T.; Raman, E.P.; Klimov, D.K. Molecular dynamics simulations of anti-aggregation effect of ibuprofen. *Biophys. J.,* **2010**, *98*(11), 2662-2670.

[49] Kim, S.; Chang, W.E.; Kumar, R.; Klimov, D.K. Naproxen interferes with the assembly of Aβ oligomers implicated in Alzheimer's disease. *Biophys. J.,* **2011**, *100*(8), 2024-2032.

[50] Zhu, B.-Y.; Cheng, Y.; Li, G.-B.; Yang, S.-Y.; Zhang, Z.-R. Synthesis and evaluation of styrylpyran fluorophores for noninvasive detection of cerebral β-amyloid deposits. *Bioorg. Med. Chem.,* **2016**.

[51] Tjernberg, L.O.; Callaway, D.J.; Tjernberg, A.; Hahne, S.; Lilliehöök, C.; Terenius, L.; Thyberg, J.; Nordstedt, C. A molecular model of Alzheimer amyloid β-peptide fibril formation. *J. Biol. Chem.,* **1999**, *274*(18), 12619-12625.

[52] Tjernberg, L.O.; Näslund, J.; Lindqvist, F.; Johansson, J.; Karlström, A.R.; Thyberg, J.; Terenius, L.; Nordstedt, C. Arrest of-amyloid fibril formation by a pentapeptide ligand. *J. Biol. Chem.,* **1996**, *271* (15), 8545-8548.

[53] Lührs, T.; Ritter, C.; Adrian, M.; Riek-Loher, D.; Bohrmann, B.; Döbeli, H.; Schubert, D.; Riek, R. 3D structure of Alzheimer's amyloid-β (1–42) fibrils. *Proc. Natl. Acad. Sci. U. S. A.,* **2005**, *102* (48), 17342-17347.

[54] Bjelic, S.; Nervall, M.; Gutiérrez-de-Terán, H.; Ersmark, K.; Hallberg, A.; Åqvist, J. Computational inhibitor design against malaria plasmepsins. *Cell. Mol. Life Sci.,* **2007**, *64*(17), 2285-2305.

[55] Oddo, S.; Caccamo, A.; Shepherd, J.D.; Murphy, M.P.; Golde, T.E.; Kayed, R.; Metherate, R.; Mattson, M.P.; Akbari, Y.; LaFerla, F.M. Triple-transgenic model of Alzheimer's disease with plaques and tangles: Intracellular Abeta and synaptic dysfunction. *Neuron,* **2003**, *39*(3), 409-21.

[56] Cline, G.W.; Hanna, S.B. Kinetics and mechanisms of the aminolysis of N-hydroxysuccinimide esters in aqueous buffers. *J. Org. Chem.,* **1988**, *53*(15), 3583-3586.

[57] Choi, S.R.; Golding, G.; Zhuang, Z.; Zhang, W.; Lim, N.; Hefti, F.; Benedum, T.E.; Kilbourn, M.R.; Skovronsky, D.; Kung, H.F. Preclinical properties of 18F-AV-45: A PET agent for Aβ plaques in the brain. *J. Nucl. Med.,* **2009**, *50*(11), 1887-1894.

[58] Klunk, W.E.; Lopresti, B.J.; Ikonomovic, M.D.; Lefterov, I.M.; Koldamova, R.P.; Abrahamson, E.E.; Debnath, M.L.; Holt, D.P.; Huang, G.-f.; Shao, L. Binding of the positron emission tomography tracer Pittsburgh compound-B reflects the amount of amyloid-β in Alzheimer's disease brain but not in transgenic mouse brain. *J. Neurosci.,* **2005**, *25*(46), 10598-10606.

[59] FDA Application number: 203137Orig1s000. Vizamyl. https://www.accessdata.fda.gov/drugsatfda_docs/nda/2013/203137 Orig1s000MedR.pdf.

[60] FDA Application number: 204677Orig1s000. Florbetaben. https://www.accessdata.fda.gov/drugsatfda_docs/nda/2014/204677 Orig1s000PharmR.pdf.

[61] Mathis, C.A.; Wang, Y.; Holt, D.P.; Huang, G.-F.; Debnath, M.L.; Klunk, W.E. Synthesis and evaluation of ¹¹C-labeled 6-substituted 2-arylbenzothiazoles as amyloid imaging agents. *J. Med. Chem.,* **2003**, *46*(13), 2740-2754.

[62] Choi, S.R.; Golding, G.; Zhuang, Z.; Zhang, W.; Lim, N.; Hefti, F.; Benedum, T.E.; Kilbourn, M.R.; Skovronsky, D.; Kung, H.F. Preclinical properties of ¹⁸F-AV-45: A PET agent for Aβ plaques in the brain. *J. Nucl. Med.,* **2009**, *50*(11), 1887-1894.

[63] Sundaram, G.S.; Dhavale, D.; Prior, J.L.; Sivapackiam, J.; Laforest, R.; Kotzbauer, P.; Sharma, V. Synthesis, characterization, and preclinical validation of a PET radiopharmaceutical for interrogating Aβ (β-amyloid) plaques in Alzheimer's disease. *EJNMMI Res.,* **2015**, *5*(1), 33-46.

[64] Heurling, K.; Leuzy, A.; Zimmer, E.R.; Lubberink, M.; Nordberg, A. Imaging β-amyloid using [¹⁸F] flutemetamol positron emission tomography: From dosimetry to clinical diagnosis. *Eur. J. Nucl. Med. Mol. Imaging,* **2016**, *43* (2), 362-373.

[65] Zhang, W.; Oya, S.; Kung, M.-P.; Hou, C.; Maier, D.L.; Kung, H.F. F-18 polyethyleneglycol stilbenes as PET imaging agents targeting Aβ aggregates in the brain. *Nucl. Med. Biol.,* **2005**, *32* (8), 799-809.

[66] Sundaram, G.S.; Dhavale, D.; Prior, J.L.; Sivapackiam, J.; Laforest, R.; Kotzbauer, P.; Sharma, V. Synthesis, characterization, and preclinical validation of a PET radiopharmaceutical for interrogating Aβ (β-amyloid) plaques in Alzheimer's disease. *EJNMMI Res.,* **2015**, *5* (1), 33.

[67] Rosen, W.G.; Mohs, R.C.; Davis, K.L. A new rating scale for Alzheimer's disease. *Am. J. Psychiatry,* **1984**, *141* (11), 1356-64.

[68] Ouyang, Y.; Tinianow, J.N.; Cherry, S.R.; Marik, J. Evaluation of 2-[18F] fluoroacetate kinetics in rodent models of cerebral hypoxia–ischemia. *J. Cereb. Blood Flow Metab.,* **2014**, *34* (5), 836-844.